Proceedings of the ASME 2012 Pressure Vessels & Piping Division Conference
PVP2012
July 15-19, 2012, Toronto, Ontario, Canada

PVP2012-78156

MITIGATION OF DISTORTION IN AN EDGE-WELDED BAR BY OPTIMIZATION CONTROL OF THE WELDING CURRENT AND SPEED PROFILE DURING WELDING

Mahyar Asadi

Mechanical Eng. Dept.
the University of Ottawa
Ottawa, Ontario, K1N 6N5
Canada
masadi@uottawa.ca

John A. Goldak *

Mechanical and Aerospace Eng. Dept.
Carleton University
Ottawa, Ontario, K1S 5B6
Canada
jgoldak@mrco2.carleton.ca

Christopher Bayley

DRDC Atlantic,
Dockyard Laboratory Pacific
CFB Esquimalt, Building 199(D)
PO Box 17000 Stn Forces
Victoria, BC, Victoria
Canada V9A 7N2
Christopher.Bayley@drdc-rddc.gc.ca

ABSTRACT

Welding distortion is usually controlled by clamping techniques that can be tack welds, pre-bending, and tension loading. Side heating or fast cooling can also mitigate the distortion in some applications. In addition to the clamping techniques, process parameters affect the distortion so that if one can control the welding process parameters, an optimized profile of such parameters could alleviate the distortion. It is shown in this paper that the distortion can be mitigated by using an optimized profile of welding current and travelling speed. These profiles keep the power per unit length of welding constant. It is shown that an increasing welding current at the beginning and the end of the welding path on an edge welded bar of Aluminum could result in a bar that is closer to flat compared to the constant welding current. Developing an optimized weld process parameter profile requires a trustable computational model to implement a control problem using a predictive model for distortion in front of the weld pool in order to adjust the welding current and speed. Unlike using a constant welding current for the full path of weld, the path length is divided into several sub-paths. For each of weld sub-path the control problem learns from the previous sub-path and tries to find the new value for the welding current and speed that minimize the distortion using predictive Computational Weld Mechanics (CWM). Final deflections of the bar are also compared between a constant welding current and optimized profile of welding current.

INTRODUCTION

The transient temperature field from the welding process drives a local thermal expansion-contraction. The strain due to this thermal expansion-contraction along with restraint of the structure and fixtures generate stress and plastic deformation that leads to residual stress and distortion. Such distortion can increase fabrication costs and residual stress can reduce the in-service life due to fatigue or corrosion failures. Therefore designers would like to minimize the distortion's harmful effects.

Welding distortion is usually controlled by various techniques that can be, for example, optimized tack welds [1], sequence pattern [2], pre-bending [3], and tension loading [4]. Side heating [5] or fast cooling [6] can also be effective in some cases if it is well-optimized. Schenk et. al. [7] conducted an adaptive clamping as an in-line technique for welding distortion mitigation by forcing the material to deform plastically locally.

A variety of mitigation techniques has been presented in the literature and they include many input parameters. Amongst them, welding process parameters, e. g., process type, weld power, and travel speed, can contribute to the part's distortion and residual stress. These parameters can vary in time or space

*Address all correspondence to this author.

of welding but they are usually defined fixed during welding time in most optimization and control applications. A comprehensive literature review on the application of several methods has been summarized by Benyounis and Olabi [8] in the area of welding. They have collected weld optimization applications including design of experiment (DOE), evolutionary algorithms, and computational network to develop a mathematical relationship between the welding process parameters and the objective function(s) of the weld joint. From the long list of research work collected by Benyounis and Olabi, a few were on the control applications to alleviate the welding distortion during the welding. Arya and Parmar [9], Murugan and Gunaraj [10], Benyounis et al. [11], and Casalino et al. [12] were some of them. Cook et. al. [13] also presented an in-line weld process control application for weld-bead profile control using Artificial Neural Network modelling. Other than spot welding, there are very few applications that mitigate the distortion or residual stress by optimizing the profile of welding process parameters adaptively during welding.

If one has the machinary to apply in-line variation to the welding process parameters such as welding current and speed during welding, then this paper shows that an adaptive control of such parameters could mitigate the distortion. This paper uses an FEM model to predict the distortion at several points along the weld path. At each point, a decision made based on the maximum distortion in the part to adjust the welding current and speed for the continuation of welding subject to the constraint that the weld power per unit length is held constant. It is shown that the final deflection can be mitigated by using such an optimized profile of welding current and speed.

CONTROL PROBLEM

From a control point of view, we have a control problem with a large time-dependent vector Q that describes the state space of our problem at the time t. The state space is governed by Computational Weld Mechanics (CWM) analysis, which is our FEM model, written as a form in Eq. 1 where u is a control vector and F is a mapping from $R^m \rightarrow R^n$. R^m is the control space and R^n is the state space. In this analysis, the vector of Q consists of the 3 components of nodal displacements and the vector u consists of welding current and speed. Therefore m and n are 29,040 (3×9680, i. e., the total number of nodes) and 2 respectively.

$$Q_t = F\left(Q_{t-1}, u_t\right) \tag{1}$$

We also define a scalar-valued function ϕ called an objective function that is to be optimized. In our problem, the objective function is the lowest maximum distortion in the part. ϕ is a function of the state , Q, and control vector u. The state , Q, is a function of the control vector u and therefore the function ϕ really depends only on u (See Eq. 2).

$$\phi\left(Q,u\right) = \phi\left(Q\left(u\right),u\right) = \phi\left(u\right) \tag{2}$$

The question that all optimization methods try to answer is how the objective function, ϕ, changes with respect to changes in the control vector u. Optimization algorithms are usually described independent of the machinery needed to evaluate the objective function.

Mapping from control space to the state space, i. e., CWM analysis, plays a critical role in the industrial applications of weld optimization problems. If the capability of such analysis exists to solve problems in a feasible time and cost, then the optimization is straight forward. A set of points in the control space can be defined in the form of a matrix in which each row defines one point in the design space and each column defines one coordinate or variable in the control space. This matrix is formally similar to a design of experiment (DOE) matrix. However, the analysis uses a deterministic model and there is no uncertainty in the solution other than truncation error and precision.

COMPUTATIONAL MODEL

An edge weld on a $1220 \times 152 \times 12.5$ mm bar shown in Fig. 1, is used in this paper for optimization of the welding current profile and speed to mitigate the distortion on the bar. The full computational model that includes thermal and stress analysis are analyzed using VrWeld software [14]. The main consideration of the model for transient thermal and stress analysis are described further in this paper. The Computational Weld Mechanics (CWM) model of this bar is validated in [15] by comparing the transient temperature, strain and deflection on this bar with the experimental data from [16]. The mesh employed is shown in Fig. 2 has 6600 8-node brick elements and 9680 nodes. This mesh is an extruded mesh along the weld path including 114 extruded elements or extrusion sections.

The material was Aluminum 5052-H32 alloy with chemical composition Al 96.7, Mg 2.5, Cr 0.25, Cu max 0.1, Fe max 0.4, Mn max 0.1, Si max 0.25, Zn max 0.1 Wt %. The temperature dependent material properties of Al 5052-H32 were given in [16] and this data was employed in this analysis. The gas metal-arc-welding process was employed to weld the specimen and the initial welding parameters were current 260 [amp], voltage 23 [v], travel speed 7.1 [mm/s], filler metal Al-4043 with 1.6 [mm] wire diameter, wire feed speed 170 [mm/s] and the shielding gas was Argon. Since this is a control problem, the value of the welding current and speed were adjusted along the weld path on the edge of the bar while the welding was progressing. The ratio of

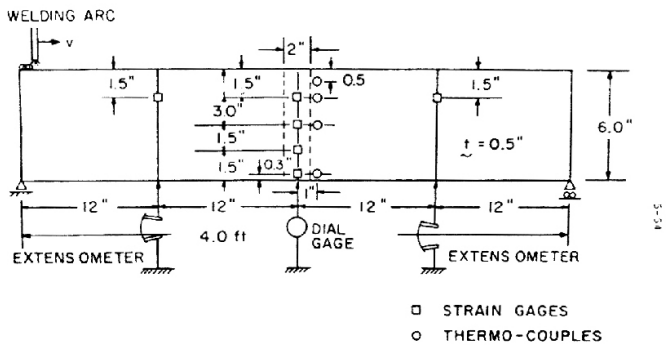

FIGURE 1: SPECIMEN VALIDATED AND USED IN THIS ANALYSIS.

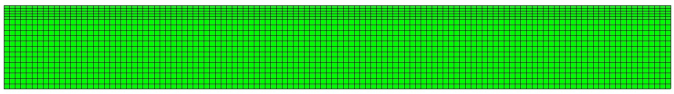

FIGURE 2: A 2D VIEW OF 3D MESH USED IN THIS ANALYSIS.

the variation in the value of the welding current and speed remained constant in order to keep the power per unit length of weld constant as it sets initially. The welding current and speed were bounded by maximum and minimum limits. The specimen was allowed to cool to ambient temperature after the welding was completed.

Thermal Analysis

A weld applies a moving local high intensity power source to the part that generates a sharp thermal profile in the weld pool, heat affected zone (HAZ) and around the weld. This causes a local change in microstructure, stress and strain state that can have a large effect on the whole structure. The 3D transient temperature is determined by solving the partial differential equation for the conservation of energy which is given in Eq. 3 for a Lagrangian or material formulation.

$$\dot{h} + \nabla \cdot (-k\nabla T) = Q \tag{3}$$

where h is the specific enthalpy, the super imposed dot denotes the derivative with respect to to time, k is the thermal conductivity, T is the temperature, and Q is the power per unit volume or the power density distribution.

Because the heat source is moving, we can define an Eulerian frame with origin at the center of the heat source. Using an Eulerian frame enables longer time steps for the weld when the

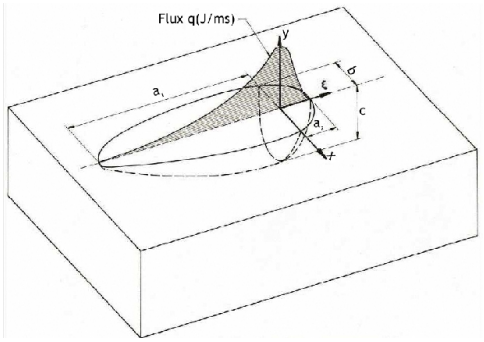

FIGURE 3: DOUBLE ELLIPSOID PARAMETERS; FRONT a_2, REAR a_1, WIDTH b, AND DEPTH c.

analysis approaches steady state. But the Eulerian frame introduces an advection term as in Eq. 4 into the FEM equation.

$$\frac{DT(X,t)}{Dt} = \frac{\partial T(x,t)}{dt} + \overrightarrow{V}.\nabla T \tag{4}$$

This term is nonlinear and hard to solve. Gu [17] implemented a weld model in the Eulerian frame. This is basically an Eulerian mesh fixed in space tied to the arc and the part moves under the arc. CWM analyses usually use a material frame for modeling where the heat source moves in discretized time as steps in series of spot welds. This frame requires sufficiently small time steps to approximate a continuous heat source. The transient heat equation can be solved by the standard Lagrangian finite element method [18]. It maps the Eulerian thermal field into the material mesh by tracking along the flow lines for each time step. Because the elements can be deformed in the forward time step, a semi-Lagrange algorithm can be used that starts from the last time step and back tracks along the flow lines to update the state.

In this analysis, the initial temperature was 300 $^{\circ}K$. The power density distribution function Q $[w/m^3]$ was the "Double Ellipsoid" heat source model [19] with the heat source sizes; front, rear, width and depth set to a_2 =8, a_1 =16, b =10 and c =8 mm (see Fig 3).

A convection boundary condition generated a boundary flux q $[w/m^2]$ on all external surfaces. This flux is computed from Eq. 5 with ambient temperature of T_{ambient} = 300 $^{\circ}K$ and convection coefficient as a function of temperature given in Eq. 6 extracted by interpolation of experimental data from [20] (Units are $[w/m^2K]$).

$$q = h_c(T - T_{\text{ambient}}) \tag{5}$$

$$h_c = 7.2 - \left(\frac{355000}{T^2}\right) + (0.001 \times T) \tag{6}$$

The time step length during welding was chosen so that the heat source travels one extruded element along the weld path on each time step. The number of elements extruded along the weld path was 114 and the analysis had 114 time step for the welding plus 45 time steps for cool-down (total of 159 time steps). Filler metal was added as the welding arc moved along the weld path, i.e., the FEM domain changed in each time step during welding. After the weld pass was completed, the time step length was increased exponentially by a factor of 1.2 per time step until a maximum user-defined cool-down time reached, and the analysis was halted. The cool-down time was 3600 seconds and the maximum temperature reached 334 $^{\circ}K$ at the end of cool-down when the analysis halted.

Stress Analysis

The stress analysis is quasi-static because inertial or dynamic forces are sufficiently small that they can be neglected. Therefore at each instant of time, the domain is in static equilibrium. However, the temperature is time dependent and therefore the thermal strain due to thermal expansion is time dependent. If microstructure evolution is included in the model, then microstructure is time dependent. When a phase changes, then the specific volume, V, or density, ρ, of the phase changes. The incremental volumetric strain tensor in a time step is $\mathbf{I}\Delta V/V$. In this paper, the evolution of microstructure was not included and the stress analysis used a time-dependent thermal strain from the thermal analysis.

In a time step, the multiplicative decomposition of the deformation gradient F can be written as $F = F_{el}F_{pl}F_{\Delta V}$. The deformation gradient due thermal expansion and phase changes is $F_{\Delta V} = \mathbf{I} + \mathbf{I}\Delta V/V$. The deformation gradient due to visco-plastic deformation is F_{pl}. The deformation gradient due to elastic deformation is $F_{el} = FF_{\Delta V}^{-1}F_{pl}^{-1}$. The reference state or initial condition for each time step is the state at the start of the time step which is constrained to be an equilibrium state.

Given the density ρ, the fourth order visco-elasto-plastic tensor D_{VP} as a 6×6 matrix, the body force b and the Green-Lagrange elastic strain $\varepsilon_{el} = (F_{el}^T F_{el} - \mathbf{I})/2$, VrWeld solves the conservation of momentum equation at the end of each time step that can be written in the form of Eq. 7 in which inertial forces, $\rho\ddot{x}$, are ignored.

$$\begin{aligned} \nabla \cdot \sigma + b &= 0 \\ \sigma &= D\varepsilon_{el} \\ \varepsilon_{el} &= (F_{el}^T F_{el} - \mathbf{I})/2 \end{aligned} \tag{7}$$

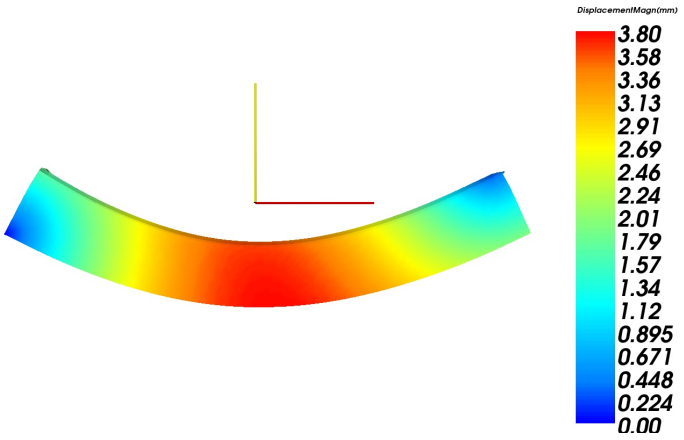

FIGURE 4: FINAL MAGNITUDE OF DISTORTION [mm](50X). RED AND YELLOW AXIS SHOW POSITIVE X AND Y DIRECTION.

This solves the associated system of partial differential equation for a visco-thermo-elasto-plastic stress-strain relationship using theory and algorithms developed by J. C. Simo and his colleagues. In each time step, the visco-thermo-elasto-plastic stress-strain algorithm begins by computing a trial elastic stress with the assumption that the visco-plastic deformation gradient is zero. If that deviatoric stress state exceeds the deformation resistance, which is similar to a yield stress, the stress relaxes towards the deformation resistance at a rate controlled by the viscosity. This stress relaxation is accompanied by a visco-plastic strain increment. Newton-Raphson iterations are performed in each time step until convergence is attained. In each Newton-Raphson iteration, the visco-elasto-plastic tensor D_{VP} is recomputed. Readers may consult with [21] for details. The initial state for each time step is assumed to be at equilibrium.

In terms of boundary condition, the part is free to deform but rigid body modes are constrained to zero. The final distortion forms a camber in the bar so that the maximum occurs in the middle of the bar as shown in Fig. 4. The maximum magnitude of Y displacement is 3.8 mm with mitigation.

OPTIMIZATION ALGORITHM

The control parameters are the welding current and travel speed. The power per unit length is constrained to be constant and equal to the initial value, i. e., 1172 [Kw/m]. This constraint also constrains variations in the welding current and speed. Therefore, the independent control vector can be either the welding current or the traveling speed. In this paper, the welding current was controlled and the traveling speed was adjusted to keep the power per unit length equal to 1172 [Kw/m].

The weld path with 114 extruded elements was divided into 19 sub-paths where each one had 6 extruded elements. This means that the control algorithm was applied every 6 time-steps during welding. The only reason for picking every 6 elements is to save CPU time and the user time to set up the projects. An automated framework is being developed to perform the user tasks and save the analysis time significantly. Such automation enables the implementation of control problem at each time step.

The control algorithm is summarized as follow:

1. Read the welding current, I, and traveling speed, S, from the last time step of the last sub-path.
2. Perturb the welding current I by $\pm\alpha\%$ and adjust S to keep the power per unit length constant.
3. Run the FEM analysis for the next sub-path using three values of the welding current; I-$\alpha\%$I, I, and I+$\alpha\%$I with adjusted S for each one.
4. Evaluate the user-defined objective function for the three analyses from the previous step and pick the best configuration.
5. Continue the analysis for the next sub-path using the picked set of I and S from the previous step.
6. Repeat at the end of the sub-path until the end of the welding path.

In this paper, α was choosen equal to 10 %, and the objective function was the maximum Y-displacement in the bar. Therefore the best pick was the lowest maximum Y-displacement. Two thresholds were considered so that the travel speed are allowed between 4.5 to 10 [mm/s]. Table 1 shows the details for each sequence of control along the weld path,as well the perturbation of the welding current, the adjusted travelling speed, and the best pick at each control sequence.

The travel distance per time step is one element, i.e, 10.7 mm per time step. Converting the time steps from Table 1 to the travelling distance, Fig. 5 shows the optimized welding current profile that mitigates the final distortion of the bar. Since there was a constrained to keep the power per unit length, the rate of variation in welding speed should be identical to the welding current keeping the power per unit length constant. Using identical variation rate for welding speed, the variation of welding speed is shown in Fig. 6.

RESULTS AND DISCUSSION

Step 4 in the control algorithm requires the user to define the objective function. In order to show an example of our definition of the best configuration which is the lowest maximum Y-displacement along the bar at each sequence, the implementation of step 4 is shown in Fig. 7 for the second sequence of the control system. This figure shows the Y-Displacements along the bar resulted from 3 different configurations of the welding

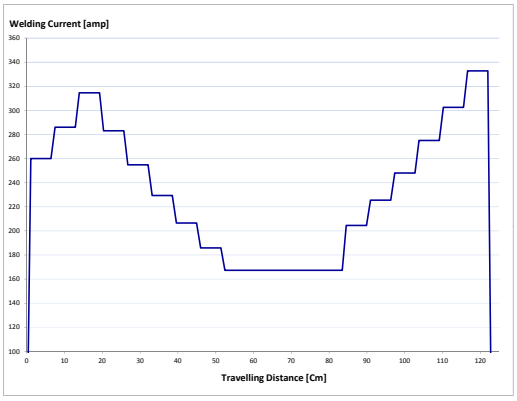

FIGURE 5: THE OPTIMIZED WELDING CURRENT PROFILE THAT MITIGATES THE FINAL DISTORTION OF THE BAR VS THE TRAVELLING DISTANCE OF WELD ON THE BAR'S TOP EDGE. THIS PROFILE SHOULD BE EMPLOYED TOGETHER WITH THE SPEED PROFILE AT FIG. 6.

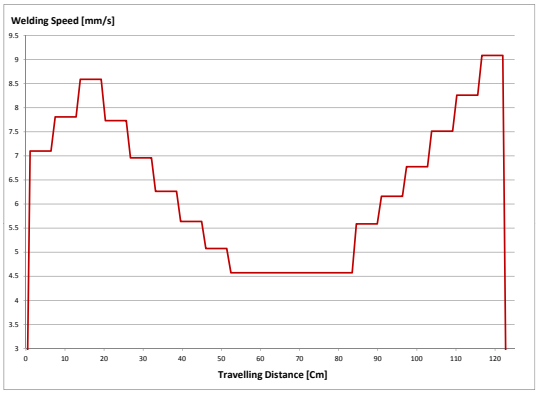

FIGURE 6: THE OPTIMIZED WELDING SPEED PROFILE THAT MITIGATES THE FINAL DISTORTION OF THE BAR VS THE TRAVELLING DISTANCE OF WELD ON THE BAR'S TOP EDGE. THIS PROFILE SHOULD BE EMPLOYED TOGETHER WITH THE CURRENT PROFILE AT FIG. 5.

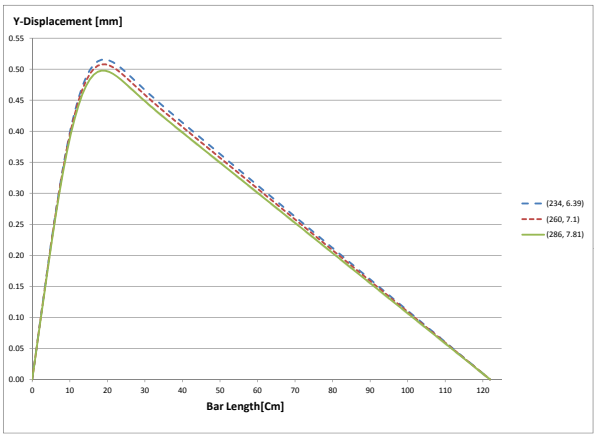

FIGURE 7: Y-DISPLACEMENT RESULTS FROM 3 DIFFERENT CONFIGURATIONS OF THE WELDING CURRENT AND SPEED THAT ARE ANALYSED AT THE SECOND SEQUENCE OF THE CONTROL SYSTEM IN ORDER TO PICK THE BEST ONE, i. e., 286 [amp] AND 7.81 [mm/s].

current and speed. The best pick then was 286 [amp] and 7.81 [mm/s].

Fig. 8 shows the Y-displacement measured after applying the best pick of each control sequence. This figure shows the transient Y-displacement along the bar when the weld pool travels on the edge of the bar. Given that the control sequence was used every 6 time steps or 64.2 [mm] of the weld pool move, the curves are the continuation of the displacement after every 64.2 [mm] of the weld pool travel.

Fig. 9 shows the final Y-displacement (after cool down) and compares the final distortion between the scenario with no mitigation technique and the scenario with controlling the welding current and speed. This comparison shows that the bar is relatively more close to flat using the process parameter control. In the case that there is no mitigation, the maximum displacement happens to be in the middle of the bar creating one big bend. Conversely, controlling the process parameters can break it into two small bends giving a final shape that is closer to a flat bar. The former scenario with two small bends would often be preferred in industrial applications rather than the a large displacement in the middle (solid blue curve vs. dotted red curve in Fig. 9).

This paper is based on computational study and the results are subject to the simplifications employed by the model. For instance, a constant arc efficiency is used, while some studies have shown that the arc efficiency can increase with the current. The assumption is that the power per unit length (or Heat Input) is kept unchanged at any configuration of weld parameters. the filler-matel feeding rate affects the power per unit length, therefore, the feeding rate should be adjusted such that the power per unit length remains unaffected.

CONCLUSION

Hamming states [22] , “the purpose of computing is insight, not numbers”.The authors believe that insight is very important in CWM. This paper takes the view that the goal of CWM is to optimize the design of weld procedures, welds and welded structures. To achieve that goal, CWM must be integrated with computational optimization.

Developing an automated framework that integrates control algorithms with Computational Weld Mechanics has a key role to practically utilize it in actual industrial problems. Such a framework saves the user time by avoiding manual tasks and organizing multiple analyses of welded structures with a minimum effort for the user(s). This also avoids human error which is very likely in a large setting and sequence of analyses in control algorithms. This automation in integration enables the users to devote more time to optimization rather than implementation and to complete the tasks in feasible time and cost.

A control algorithm was developed and used in this paper for an adaptive control of welding current and speed in order to mitigate the final deflection during welding. The comparison between the strategy with no application of control and the strategy that uses the control scheme shows the effectiveness of the control scheme. Although the bar analyzed in this paper is relatively simple structure, the control algorithm is directly applicable to any welded structure.

The CPU time was 48 minutes for the full analysis and about 2.5 minutes per sub-path. The total CPU time for running the control and simulation was about 150 minutes. However the manual implementation of this analysis took a week of expert-user time which is mostly preparation and setup. This manual preparation time can be significantly high in complex and large projects so that the analysis would become unfeasible in practice. An automated framework saves the user’s time (a week in this case) and drops the total time to the CPU (150 minutes in this case). CPU time per analysis would increase for larger more complex structures but the user’s time would change little.

ACKNOWLEDGMENT

The authors would like to thank Daniel Downey, Stanislav Tchernov and Jianguo Zhou for their support and contribution to this study.

TABLE 1: DETAILS FOR EACH SEQUENCE OF CONTROL VALUES ALONG THE WELD PATH.

Sequence No.	Time Step	I [amp], S [mm/s]	Picked
1	1-6	260, 7.1	∗
2	7-12	234, 6.39	
		260, 7.1	
		286, 7.81	∗
3	13-18	257.4, 7.029	
		286, 7.81	
		314.6, 8.591	∗
4	19-24	283.14, 7.7319	∗
		314.6, 8.591	
		346.06, 9.4501	
5	25-30	254.826, 6.95871	∗
		283.14, 7.7319	
		311.454, 8.50509	
6	31-36	229, 6.264	∗
		254.87, 6.96	
		280.357, 7.656	
7	37-42	206.46, 5.6376	∗
		229.4, 6.264	
		252.34, 6.8904	
8	43-48	185.85, 5.076	∗
		206.5, 5.64	
		227.15, 6.204	
9	49-54	167.31, 4.572	∗
		185.9, 5.08	
		204.49, 5.588	
10	55-60	167.31, 4.572	∗
		185.9, 5.08	
		204.49, 5.588	

TABLE 2: Con't

Sequence No.	Time Step	I [amp], S [mm/s]	Picked
11	61-66	167.31, 4.572	∗
		185.9, 5.08	
		204.49, 5.588	
12	67-72	167.31, 4.572	∗
		185.9, 5.08	
		204.49, 5.588	
13	73-78	167.31, 4.572	∗
		185.9, 5.08	
		204.49, 5.588	
14	79-84	167.31, 4.572	
		185.9, 5.08	
		204.49, 5.588	∗
15	85-90	184.5, 5.04	
		205, 5.6	
		225.5, 6.16	∗
16	91-96	202.95, 5.544	
		225.5, 6.16	
		248.05, 6.776	∗
17	97-102	225, 6.143	
		250, 6.83	
		275, 7.513	∗
18	103-108	247.5, 6.759	
		275, 7.51	
		302.5, 8.261	∗
19	109-114	272.25, 7.4349	
		302.5, 8.261	
		332.75, 9.0871	∗
20	114-159	0, 0	

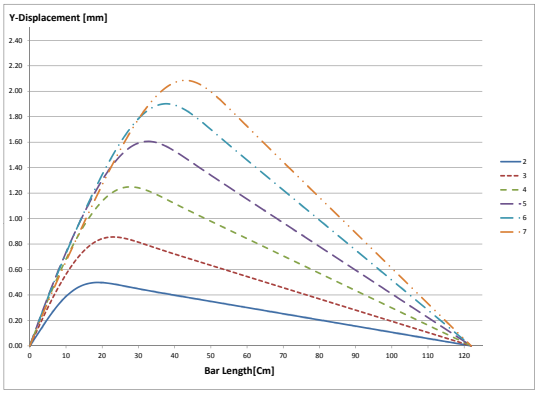

(a) Control Sequence: 1 to 7

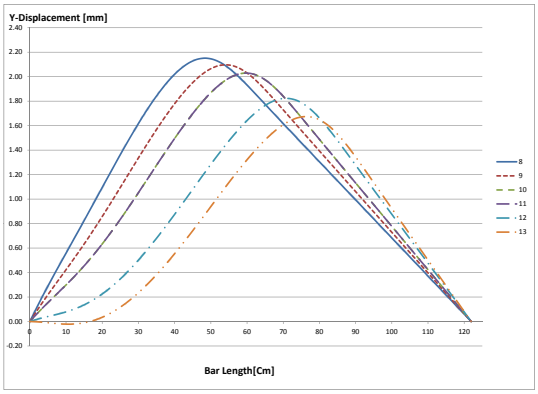

(b) Control Sequence: 8 to 13

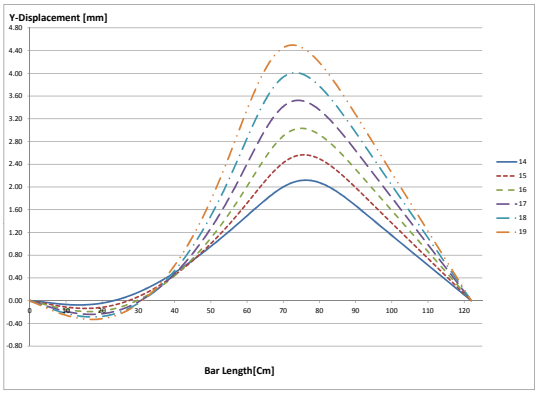

(c) Control Sequence: 14 to 19

FIGURE 8: Y-DISPLACEMENT MEASURED AT THE END OF EACH CONTROL SEQUENCE.

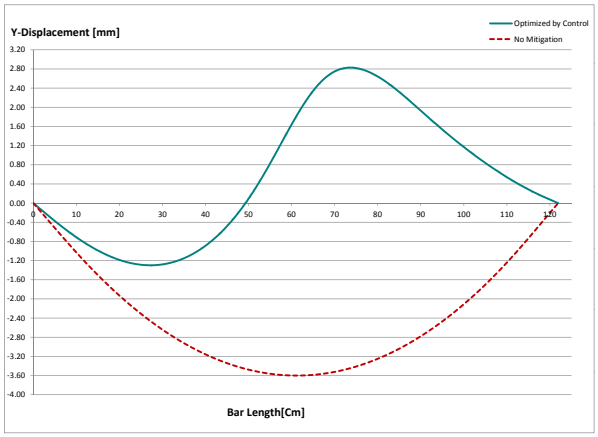

FIGURE 9: COMPARISON BETWEEN THE FINAL DISTORTION OF THE SCENARIO WITH NO MITIGATION TECHNIQUE AND THE SCENARIO WITH CONTROLLING THE WELDING CURRENT AND SPEED.

REFERENCES

[1] C. L. Tsai, S. C. Park, W. T. Cheng, Welding Distortion of a Thin-Plate Panel Structure, Welding Research Supplement, pp. 156-s - 165-s, 1999.

[2] M. Asadi, J. A. Goldak, Combinatorial Optimization of Weld Sequence by Using a Surrogate Model to Mitigate a Weld Distortion, Int'l J. of Mechanics and Material in Design, Volume 7, Number 2, 123-139, DOI: 10.1007/s 10999-011-9154-6, Springer, April 2011.

[3] M. Asadi, J. A. Goldak, Mitigation of Distortion in an Edge-Welded-Bar by Clamping Parameters, Proceeding of the International ASME 2011 Pressure Vessel and Piping Division Conference, Baltimore, Maryland, PVP2011-57955, July 17-21, 2011.

[4] J. A. Goldak, M. Asadi, The Evolution of Stress and Strain Tensors in Welds with Mitigation of Residual Stress and Distortion, Proceeding of the International ASME 2011 Pressure Vessel and Piping Division Conference, Baltimore, Maryland, PVP2011-57957, July 17-21, 2011.

[5] M. Asadi, J. A. Goldak, A Direct-Search Computational Weld Mechanics Optimization Using Least-Square Approximation, Proceeding of the International ASME 2011 Pressure Vessel and Piping Division Conference, Baltimore, Maryland, PVP2011-57960, July 17-21, 2011.

[6] T. E. Barber, F. W. Burst, H. W. Mishler, M. F. Kanninen, Controlling Residual Stresses by Heat Sink Welding, Battle Memorial Institute, Electric Power Research Institute Report NP-2159-LD, December 1981.

[7] T. Schenk, I. M. Richardson, M. Kraska, S. Ohnimus, A Study on the Influence of Clamping on Welding Distortion, Computational Materials Science, Volume 45, Issue 4, June 2009, Pages 999-1005, doi:10.1016/j.commatsci.2009.01.004

[8] K. Y. Benyounis, A. G. Olabib, Optimization of Different Welding Processes Using Statistical and Numerical Approaches - A Reference Guide, Advances in Engineering Software, Volume 39, Issue 6, June 2008, Pages 483-496, doi:10.1016/j.advengsoft.2007.03.012

[9] S. K. Arya, R. S. Parmar, Mathematical Models for Predicting Angular Distortion in CO2-Shielded Flux Cored Arc Welding, The proceedings of International Conference on Joining of Metals (JOM-3), Helsingor, Denmark (1986), pp. 240-245.

[10] V. V. Murugan, V. Gunaraj, Effects of Process Parameters on Angular Distortion of Gas Metal Arc Welded Structural Steel Plates. Weld J. AWS, November (2005), pp. 165-s-171-s.

[11] K. Y. Benyounis, A. G. Olabi, M. S. J. Hashmi, Residual Stresses Prediction for CO2 Laser Butt-Welding of 304-Stainless Steel, Applied Mechanics and Materials, Vols. 3-4 Trans Tech Publications. (2005), pp. 125-130.

[12] G. Casalino, S. J. Hu, W. Hou, Deformation Prediction and Quality Evaluation of the Gas Metal Arc Welding Butt Weld. J. Eng Manuf, 217 part B (2003), pp. 1615-1622.

[13] G. Cook, R. J. Barnett, K. Andersen, A. M. Strauss, Weld Modelling and Control Using Artificial Neural Networks. IEEE Trans Ind Appl, 31 6 (1995), pp. 1484-1491.

[14] Goldak Technology Inc., *http://www.goldaktec.com/vrweld.html*, Accessed January 2012.

[15] M. Asadi, J. A. Goldak, Challenges in Verification of CWM Software to Compute Residual Stress and Distortion in Weld, Proceeding of the ASME 2010 Pressure Vessel and Piping Division Conference, Bellevue, Washington, PVP2010-25770, July 18-22, 2010.

[16] K. Masabuchi, Analysis of Welded Structures, Section Transient Thermal Stress, pp.172 - 187, 1983.

[17] M. Gu, J. A, Goldak, Steady State Thermal Analysis of Welds with Filler Metal Addition, Can Metal. Q., Volume 32, pp. 49-55, 1993.

[18] O. Zienkiewicz, R. Taylor, The Finite Element Method, Fourth Edition, Volume 2, McGraw-Hill, 1989.

[19] J. A. Goldak, A. Chakravarti, M. J. Bibby, A New Finite Element Model for Welding Heat Sources, Trans. AIME.186 Vol. 15B, pp. 299-305, June 1984, .

[20] J. D. Francis, Welding Simulations of Aluminum Alloy Joints by Finite Element Analysis, M. Sc. thesis Virginia Polytechnic Institute and State University, April 2002.

[21] J. C. Simo, Numerical Analysis of Classical Plasticity, Handbook for Numerical Analysis, Volume VI, ed. by P.G. Ciarlet and J.J. Lions, Elsevier, Amsterdam, 1998.

[22] R. W. Hamming, Numerical Methods for Scientists and Engineers, Book by Dover Publications, ISBN: 9780486652412, New York, 1987.